ResearchGate

See discussions, stats, and author profiles for this publication at: https://www.researchgate.net/publication/336997423

The effect of grain boundary structure on the intergranular degradation behavior of solution annealed Alloy 690 in high temperature, hydrogenated water

Article *in* Acta Materialia · October 2019

DOI: 10.1016/j.actamat.2019.10.041

CITATIONS
2

READS
83

2 authors, including:

Wenjun Kuang
University of Michigan
34 PUBLICATIONS **385** CITATIONS

SEE PROFILE

All content following this page was uploaded by Wenjun Kuang on 12 November 2019.

The user has requested enhancement of the downloaded file.

Acta Materialia 182 (2020) 120–130

Contents lists available at ScienceDirect

Acta Materialia

journal homepage: www.elsevier.com/locate/actamat

Full length article

The effect of grain boundary structure on the intergranular degradation behavior of solution annealed alloy 690 in high temperature, hydrogenated water

Wenjun Kuang[a,b,*], Gary S. Was[b]

[a] Center for Advancing Materials Performance from the Nanoscale (CAMP-Nano), State Key Laboratory for Mechanical Behavior of Materials, Xi'an Jiaotong University, Xi'an 710049, PR China
[b] Department of Nuclear Engineering and Radiological Sciences, University of Michigan, Ann Arbor, MI 48109, United States

ARTICLE INFO

Article history:
Received 15 July 2019
Revised 27 September 2019
Accepted 24 October 2019
Available online 30 October 2019

Keywords:
Nickel alloy
STEM
Grain boundary diffusion
Stress-corrosion cracking
Grain boundary migration

ABSTRACT

The environmental degradation of four different types of grain boundaries were investigated on alloy 690 following slow strain rate tensile tests in 360°C hydrogenated water. Random high angle boundaries (RHABs) support fast Cr diffusion that promotes the formation of a continuous surface oxide film and grain boundary migration. Surprisingly, coherent twin boundaries (CTBs) are susceptible to intergranular oxidation and do not exhibit Cr diffusion or grain boundary migration. When CTBs are changed to transformed twin boundaries (TTBs) by cold work, they behave like RHABs. Finally, incoherent twin boundaries (ITBs) undergo intergranular oxidation with limited Cr depletion but no boundary migration beyond the oxide. The Cr diffusivity along grain boundary in this alloy is directly related to the density of coincident site in the grain boundary plane and determines the morphology of oxide formed near the grain boundary. CTBs are still highly resistant to stress corrosion cracking (SCC) due to the semi-coherent interface between the intergranular chromia and grain matrix. In contrast, the intergranular oxides formed along RHABs inherit highly-disordered boundary structure from the original grain boundaries and show much higher SCC susceptibility. The grain boundary structure dependence of SCC resistance should be understood from its effects on solute diffusivity, structure of intergranular oxide and the local stress-strain state.

© 2019 Acta Materialia Inc. Published by Elsevier Ltd. All rights reserved.

1. Introduction

Nickel base alloy 690 is an important structural material in pressurized water reactors (PWRs) thanks to its higher stress corrosion cracking (SCC) resistance than alloy 600 [1–3]. Its performance lives up to its reputation thus far as no incidence of SCC has been reported in a nuclear power plant since its introduction in the late 1980s. However, the reliability of alloy 690 is still concerned because the designed life time of a PWR is around 40 years with the possibility of further life extension. Moreover, the crack growth rate tests indicate that alloy 690 is still susceptible to SCC propagation [4], especially when the material has been cold worked [5,6]. Extensive data also shows that this material is susceptible to SCC initiation in constant extension rate tensile (CERT) tests [7–12]. Some other work indicates that intergranular crack initiation on thermally treated and cold worked alloy 690 can result from creep cavitation in constant load tests [13,14].

SCC of Fe-Cr-Ni alloys in PWR primary water is predominantly an intergranular process. The high-resolution characterization of SCC initiation in alloy 690 [15] suggests that a protective Cr_2O_3 layer forms over random high angle grain boundary (RHAB) via fast diffusion of Cr along the grain boundary, which results in a diffusion-induced grain boundary migration (DIGM) zone. Breakdown of the surface Cr_2O_3 layer under dynamic straining and oxidation down the grain boundary or into the DIGM zone are necessary steps in the crack initiation process. Kuang et al. [16] analyzed the microstructure of cracked grain boundaries in alloy 690 after a CERT test in high temperature hydrogenated water and observed a continuous Cr_2O_3 layer and a deep DIGM zone beyond a stagnant crack while the active crack is preceded by porous oxide in the DIGM zone. So, both crack initiation and propagation are closely related to Cr diffusion along the grain boundary to form an oxide above or along the grain boundary. Therefore, grain boundary structure should play an important role in this degradation process, yet it is not well understood.

* Corresponding author at: Center for Advancing Materials Performance from the Nanoscale (CAMP-Nano), State Key Laboratory for Mechanical Behavior of Materials, Xi'an Jiaotong University, Xi'an 710049, PR China.
E-mail address: wjkuang66@xjtu.edu.cn (W. Kuang).

https://doi.org/10.1016/j.actamat.2019.10.041
1359-6454/© 2019 Acta Materialia Inc. Published by Elsevier Ltd. All rights reserved.

It has been reported that twin boundaries are highly resistant to environmental degradations such as oxidation and cracking. Yamaura et al. [17] studied the intergranular oxidation of Ni-40 at.% Fe in high temperature gases and found that the twin boundaries were highly resistant to oxidation when the deviation angle is less than 10°. The work from Lim et al. [18] also suggested that in simulated PWR primary water, twin boundaries in alloy 600 were free of oxidation while RHABs were oxidized. Pan et al. [19] reported that twin boundaries of alloy X-750 did not crack regardless of the boundary plane crystal orientation after a crack propagation test in 360 °C deaerated water. Gertsman and Bruemmer [20] found that consistently, only twin boundaries were crack-resistant in alloy 600 and Fe-base austenitic stainless steels in high temperature water although they were not completely immune. Leonard et al. [21] analyzed SCC cracks in alloy 718 leaf springs after service in PWRs and found that the cracking occurred primarily along RHABs while low-angle grain boundaries and twin boundaries were much more resistant to crack propagation. More recently, Kuang et al. [22] studied the effects of cold rolling on the structure and SCC behavior of twin boundary in alloy 690 in 360 °C hydrogenated water and found that the twin boundaries were resistant to cracking while the transformed twin boundaries (TTBs) induced by cold rolling had a susceptibility to cracking similar to that of RHABs. Interestingly, twin boundaries exhibited intergranular oxidation while TTBs, and RHABs were free of oxidation prior to cracking. It seems that the twin boundaries of alloy 690 have surprisingly different oxidation susceptibility than those of other alloys. The twin boundaries of alloy 690 are still crack-resistant although they are prone to intergranular oxidation, while the TTBs and other RHABs are susceptible to cracking which yet form a protective oxide layer over the grain boundary initially [7,23]. This paradox serves to stimulate further efforts to study how the grain boundary structure affects the microstructure of intergranular oxides and thus the SCC susceptibility.

This work is focused on the degradation behaviors (oxidation and boundary migration) of different grain boundaries prior to crack initiation. Four different types of grain boundaries, namely RHAB, coherent twin boundary (CTB), incoherent twin boundary (ITB), and TTB were investigated on alloy 690 after CERT testing in 360 °C hydrogenated water. The microstructures and elemental compositions of intergranular oxides and GB migration zones were examined. The effects of grain boundary structure on the intergranular degradation behavior and SCC resistance were discussed in light of these results.

2. Experimental

2.1. Material

The chemical composition of alloy 690 studied in this work is 57.6 wt.% Ni, 32.7% Cr, 8.64% Fe, 0.25% Mn, 0.315% Al, 0.08% Si and 0.02% C. The material block was hot rolled to an 8 mm-thick sheet at around 1100 °C and then solution annealed (SA) at 1100 °C for 1 h and water quenched. Some of the stock was cold rolled (CR) to 20% thickness reduction. Round tensile bars were made with the sample axis along the cold rolled direction as described in a previous study [12]. The tensile bar is about 20 mm in gauge length and 2 mm in diameter. The gauge section of tensile bar was mechanically abraded up to 4000 grit and electropolished for 30 s at 30 V in a solution of 10% (volume fraction) perchloric acid in methanol at −30 °C. The samples were cleaned alternately with methanol and acetone immediately after electropolishing. The microstructure analysis showed that there were some small (average ~100 nm in diameter), sparse carbides on the grain boundaries which showed no sign of migration [16].

2.2. Apparatus and methodology

The CERT test was performed in 360 °C high purity water containing 18 cm^3 (STP) H_2/kg H_2O in a refreshed stainless steel autoclave. The samples were loaded to just below the yield point at a rate of 1.24×10^{-5} s^{-1} after the environment parameters were stabilized and then strained at 1×10^{-8} s^{-1} as in previous procedures [22,24,25]. One SA tensile bar was uniformly strained to 1.78% plastic strain after a total test time of 564 h. A CR tensile bar was strained to failure after a total test time of 1650 h. The uniform strain measured on the CR tensile bar was 1.90%. The crack measurement from these two samples has been provided in our previous work [22].

The grain boundaries were first examined using scanning electron microscope (SEM). The plan view images of the grain boundaries were taken after the horizontal direction was aligned with the loading axis. Cross section lamellas of grain boundaries were prepared using focused ion beam (FIB) milling on a FEI Helios Nanolab 650. An 8 × 1.5 µm section across the sampled grain boundary was first coated with ~3 µm thick Pt layer. Then a lamella of 4 µm in depth was trenched out. The lamella was lift out, attached to a Cu grid and gradually milled to ~100 nm thick with a final ion beam current of 80 pA. Both coherent and incoherent twin boundaries and RHABs were sampled from the SA tensile bar. TTBs and RHABs were sampled from the CR tensile bar. The structures of twin boundaries were confirmed with transmission electron microscopy (TEM) on a JEOL 3011 microscope. The elemental composition was analyzed with an energy dispersive spectroscopy (EDS) X-ray detector system in a scanning transmission electron microscope (STEM) JEOL 2100. High resolution images of oxides and GB migration zone were taken using a JEOL 3100R05 which is equipped with high angle annular dark-field (HAADF) detector. Fast Fourier Transformation (FFT) was used to analyze the high-resolution images.

3. Results

Four different types of grain boundaries (RHAB, CTB, ITB and TTB) have been sampled and examined in this work. Those sampled grain boundaries didn't show crack initiation. The microstructure features from each grain boundary type will be presented separately. Fig. 1 shows the SEM image of the sampled grain boundaries from the SA sample. The oxide particles formed within a single grain show similar shape and orientation but with different sizes. They are $NiFe_2O_4$ spinel oxides that grew by precipitation of cations from solution [25–28] and maintained a cube-on-cube relationship with the underlying matrix [25]. The grain boundaries can be easily located using the change in morphology of the spinel particles. For CTBs, they normally appear as pairs of straight lines

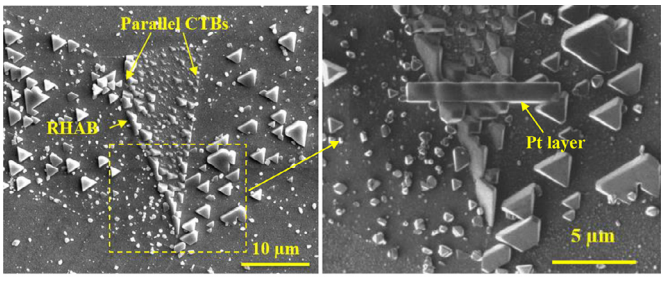

Fig. 1. (a) SEM image of sampled grain boundaries from solution annealed alloy 690, strained to 1.78% at 1×10^{-8}/s in 360 °C hydrogenated water after 564 h (from Ref. [15] with the permission of Elsevier), (b) enlarged image from the framed area on (a) showing the FIB cutting position.

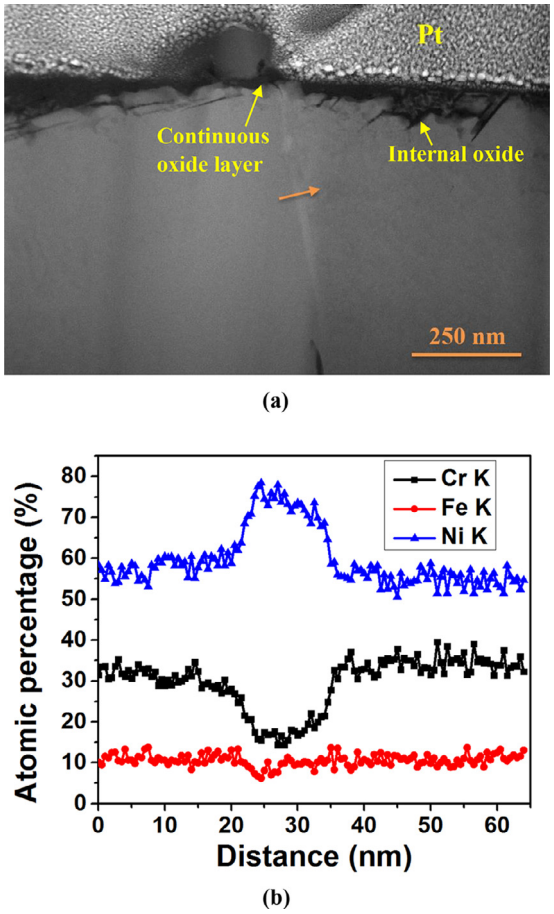

Fig. 2. (a) STEM-HAADF image of the cross section of RHAB from solution annealed alloy 690, strained to 1.78% at 1×10^{-8}/s in 360 °C hydrogenated water after 564 h and (b) EDS profile along the arrow in (a) (from Ref. [15] with the permission of Elsevier).

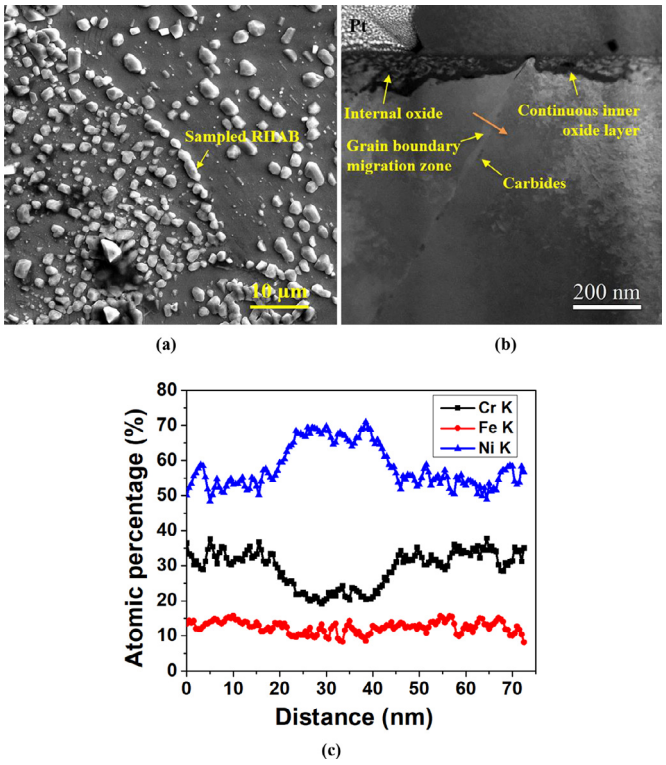

Fig. 3. (a) SEM image of the sampled RHAB in cold rolled alloy 690, strained to 1.90% at 1×10^{-8}/s in 360 °C hydrogenated water after 1650 h, (b) STEM-HAADF image of the cross section of sampled RHAB and (c) EDS profile along the arrow in (b).

across the parent grains, as shown in Fig. 1a. Both a RHAB and a CTB were sampled in a single FIB lamella (Fig. 1b). The results from the RHAB will be presented first.

3.1. Random high angle grain boundaries (RHABs)

Fig. 2a shows a STEM-HAADF image of the cross section of a RHAB. There is a layer of oxide on the surface which appears dark in the dark field image due to its lower mass density. The oxide in the grain matrix is discontinuous and appears as penetrative filaments. Those filaments are Cr_2O_3 developing along the most widely spaced lattice planes of the matrix [25]. As it approaches the grain boundary, the oxide volume fraction gets higher and the oxide layer gets thinner. There is thin a slab of bright area along the grain boundary that corresponds to the grain boundary migration zone which has been previously observed in this alloy [16,23,29]. The migration zone appears brighter than the matrix in dark field due to its higher average Z number, which in this instance implies a higher Ni content. The EDS profile along the arrow across the migration zone in Fig. 2a confirms that this zone is enriched in Ni (up to 80 at.%) and depleted in Cr (down to 15 at.%) (Fig. 2b).

A RHAB was also sampled from the CR tensile bar. The plan view of the sampled grain boundary is shown in Fig. 3a. The STEM-HAADF image of the cross section in Fig. 3b also shows discontinuous internal oxide in the matrix. The depth of internal oxide decreases as it approaches the grain boundary. The oxide layer on top of the grain boundary is continuous and extends into both grains as an inner oxide layer. This grain boundary also shows a migration zone in which the original grain boundary location is highlighted by small carbides. The EDS profile along the orange arrow in Fig. 3b confirms that the migration zone is depleted in Cr and enriched in Ni (Fig. 3c). It should be noted that the EDS scan line avoids the carbides, so those small carbides have negligible effects on the elemental profile.

3.2. Coherent twin boundary (CTB)

The cross section of the sampled CTB on Fig. 1 is shown in Fig. 4a. The transmission electron diffraction pattern of the boundary confirms that it is a CTB (Fig. 4b). From Fig. 4a, the twin boundary shows totally different features from the RHAB. There is no continuous oxide film over the twin boundary and the internal oxide depth barely changes as it approaches the boundary. Moreover, an oxide filament penetrates along the straight twin boundary and there is no sign of boundary migration. The intergranular oxidation depth is comparable to the internal oxidation depths in the neighboring grains (Fig. 4a). The EDS line scan across the thin intergranular oxide indicates that the oxide is highly enriched in Cr and depleted in Ni and Fe (Fig. 4c). The line profile across the boundary beyond the intergranular oxide shows a uniform elemental distribution with no sign of Cr depletion (Fig. 4d), indicating that there is no grain boundary migration zone.

The intergranular oxide along the CTB was further analyzed through high resolution imaging. Fig. 5a shows the STEM-HADDF of the same CTB. The sample was flipped over compared to Fig. 4a. The high-resolution images were taken with both grains titled to the common ⟨110⟩ zone axis, so that the orientation relationship between the oxide and the matrix can be clearly revealed. Fig. 5b-d were taken from the corresponding selected areas on Fig. 5a.

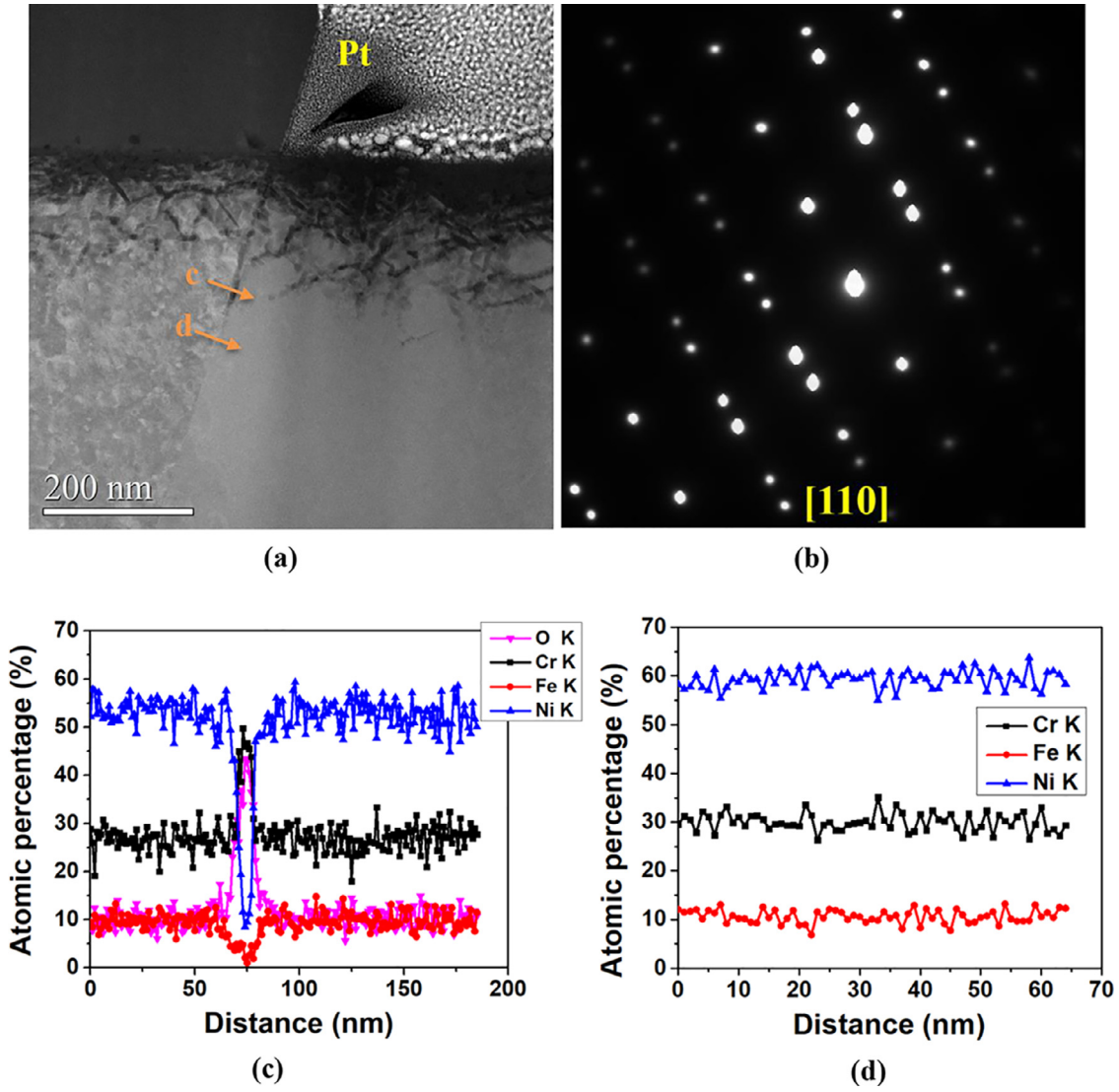

Fig. 4. (a) STEM-HAADF and (b) diffraction pattern of the sampled twin boundary from solution annealed alloy 690, strained to 1.78% at 1×10^{-8}/s in 360 °C hydrogenated water after 564 h; (c), (d) EDS profiles along the arrows in (a).

The boundary position is marked with a dashed line based on the change of lattice orientation. The unoxidized part of the boundary shows coherency between the neighboring grains (Fig. 5c and d), confirming it is a CTB. The oxide shows a corundum structure which is identified as Cr_2O_3 given that it is enriched in Cr (Fig. 4c). The chromia exhibits a rigid orientation relationship with either grain: Cr_2O_3 {006} // substrate {111}, $Cr_2O_3\langle 210\rangle$ // substrate ⟨110⟩. The same orientation relationship has also been reported to exist between internal Cr_2O_3 and grain matrix [16,25,30]. The dominant Cr_2O_3 filament grows into both grains and maintains semi-coherency with both grains along the {111} boundary plane (Fig. 5b and 5c). As shown in Fig. 5d, some Cr_2O_3 platelets maintain semi-coherency and shows a rigid orientation relationship with one of the grains.

3.3. Incoherent twin boundaries (ITBs)

Two ITBs from the SA sample were investigated. The ITB typically appears as a short segment between two parallel CTBs, like the sampled ITB shown in Fig. 6a. The FIB lamella was analyzed in TEM so as to confirm that it is indeed an ITB. The bright field image is shown in Fig. 6b and the corresponding diffraction pattern is shown in Fig. 6c. There is a zag on the boundary trace. The straight part of grain boundary near the surface (marked with a dashed line in Fig. 6b) was studied as only this part is subject to degradation. The ⟨114⟩ zone axis of the upper grain is parallel to the ⟨110⟩ zone axis of the lower grain (Fig. 6c). If it is a CTB, the grain boundary trace in Fig. 6b should be parallel to the common [220]* direction in the diffraction pattern (Fig. 6c). Fig. 6a and 6b shows that it is not, confirming that it is an ITB. Fig. 7a shows the STEM-HAADF image of the grain boundary cross section. Similar to the CTB shown in Fig. 4a, this incoherent boundary does not form a continuous surface oxide layer over the boundary either. The depths of internal oxide in both grain matrixes barely change in proximity to the boundary. EDS point analysis was performed on the intergranular oxide and the results show that the dominant elements are Cr and O with an atomic ratio around 2:3, indicating that the oxide is Cr_2O_3. The intergranular oxidation depth is comparable to the internal oxidation depths in the neighboring grains (Fig. 7a). The grain boundary beyond the intergranular oxide is still straight (Fig. 7b), suggesting that it did not migrate. Interestingly, the EDS line profile along the arrow across the boundary (Fig. 7b) shows that Cr is depleted while Ni is enriched near the boundary (Fig. 7c). High-resolution images were taken from the framed

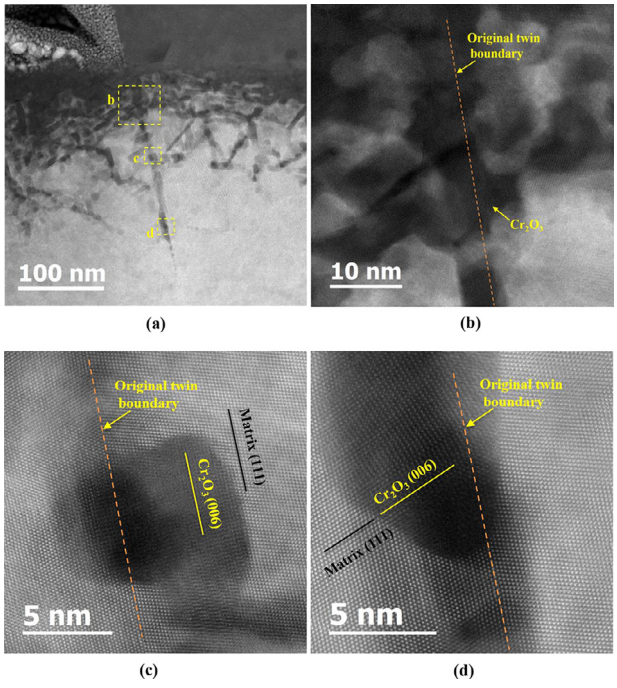

Fig. 5. (a) STEM-HAADF image of the sampled coherent twin boundary from solution annealed alloy 690, strained to 1.78% at 1×10^{-8}/s in 360 °C hydrogenated water after 564 h and (b-d) high resolution images from the framed areas on a.

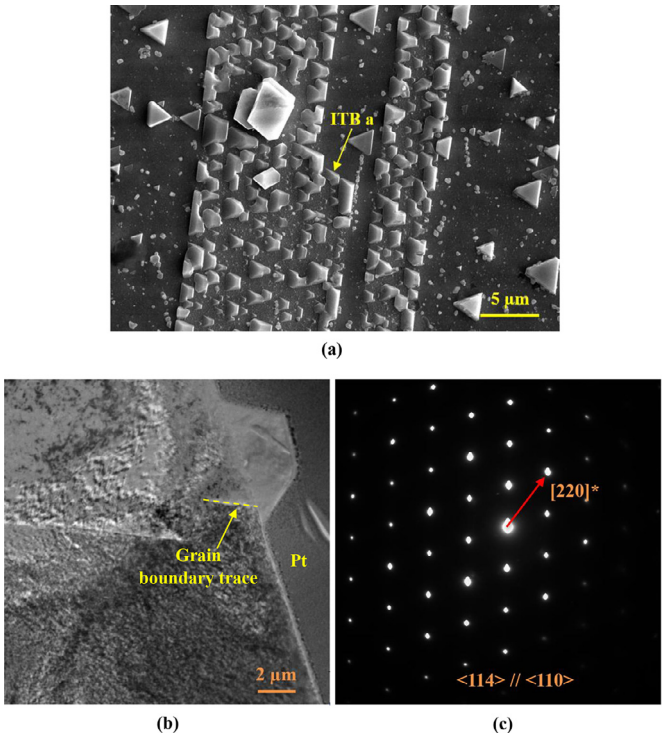

Fig. 6. (a) SEM image of sampled incoherent twin boundary a from solution annealed alloy 690, strained to 1.78% at 1×10^{-8}/s in 360 ° hydrogenated water after 564 h, (b) TEM micrograph of the cross section and (c) diffraction pattern of the grain boundary.

areas on Fig. 7b and are shown in Fig. 8. The original grain boundary position was identified based on the change of the orientation of the intergranular oxide or grain matrix in the bright field images (Fig. 8 a2 and b2). From Fig. 8 a1, the local area along the original grain boundary appears darker than the surrounding Cr_2O_3 oxide, indicating that this local area has lower average Z or higher porosity. Given that the surrounding Cr_2O_3 oxide has the lowest average Z number among the formed oxides here, the darker interface area is probably porous. The corresponding bright field image shows a narrow and disordered region along the original grain boundary (Fig. 8 a2). So, the interface between the intergranular oxides formed along the ITB is disordered and probably porous. The tip of the intergranular oxide is amorphous as it shows no lattice structure (Fig. 8 b2), and the grain boundary beyond the oxide is still straight.

Fig. 9a shows the plan view of ITB b sampled from the SA tensile bar. Similar to ITB a (Fig. 6a), this boundary also appears as a short section between two parallel CTBs. The TEM micrograph of the cross section shows that the boundary trace is straight (Fig. 9b). The corresponding diffraction pattern was taken when the right grain was titled to ⟨110⟩ zone axis and the left grain was at ⟨114⟩ zone axis (Fig. 9c). The grain boundary trace is not parallel to the common [220]* direction, confirming that this twin boundary is incoherent. From the STEM-HAADF image (Fig. 9d), penetrative oxide forms along the boundary and the depth of internal oxide does not change as it approaches the boundary in both grains. The boundary beyond the intergranular oxide is still straight and shows no sign of migration. The EDS line profile along the arrow in Fig. 9d shows depletion of Cr and enrichment of Ni near the grain boundary (Fig. 9e). These results are very consistent with those from ITB a.

3.4. Transformed twin boundaries (TTBs)

Two TTBs were studied from the CR sample. These grain boundaries were transformed from CTBs during cold rolling and appears as parallel boundaries across the parent grains [22], as shown in Fig. 10a. The STEM-HAADF image of the cross section shows a continuous oxide layer over sampled TTB a (Fig. 10b). The internal oxide in the right grain gets thinner and the volume fraction gets higher as it approaches the boundary. The original boundary was marked with a dashed line. The boundary migrated in both directions from the original position. The EDS line profiles along arrows c and d in Fig. 10b confirm Cr depletion and Ni enrichment in the boundary migration zone (Figs. 10c and d). Thus, similar to RHABs, TTBs can also support the formation of a continuous oxide layer on the surface and are subject to migration.

Fig. 11a shows the plan view of sampled TTB b which is parallel to neighboring TTBs. From the STEM-HAADF image of the cross section (Fig. 11b), there is a hole on the top which was cut during the final FIB thinning. The original grain boundary is marked with a broken black line and the migrated boundary is represented by a solid white line. The internal oxide in the left grain decreases in depth near the boundary and the volume fraction gets higher above the grain boundary. The EDS line profile across the migration zone (along the arrow in Fig. 11b) confirms that this zone is enriched in Ni and depleted in Cr (Fig. 11c). In summary, similar to the RHAB, both the sampled TTBs show formation of continuous oxide above the boundary and grain boundary migration beneath the surface.

4. Discussion

The above results show that different types of grain boundaries behave differently during exposure to high temperature hydrogenated water. The intergranular degradation process is dictated by the grain boundary structure. The effects of grain boundary structure on its degradation will be discussed with respect to solute diffusivity, the microstructure of the intergranular oxide, and the intergranular SCC resistance.

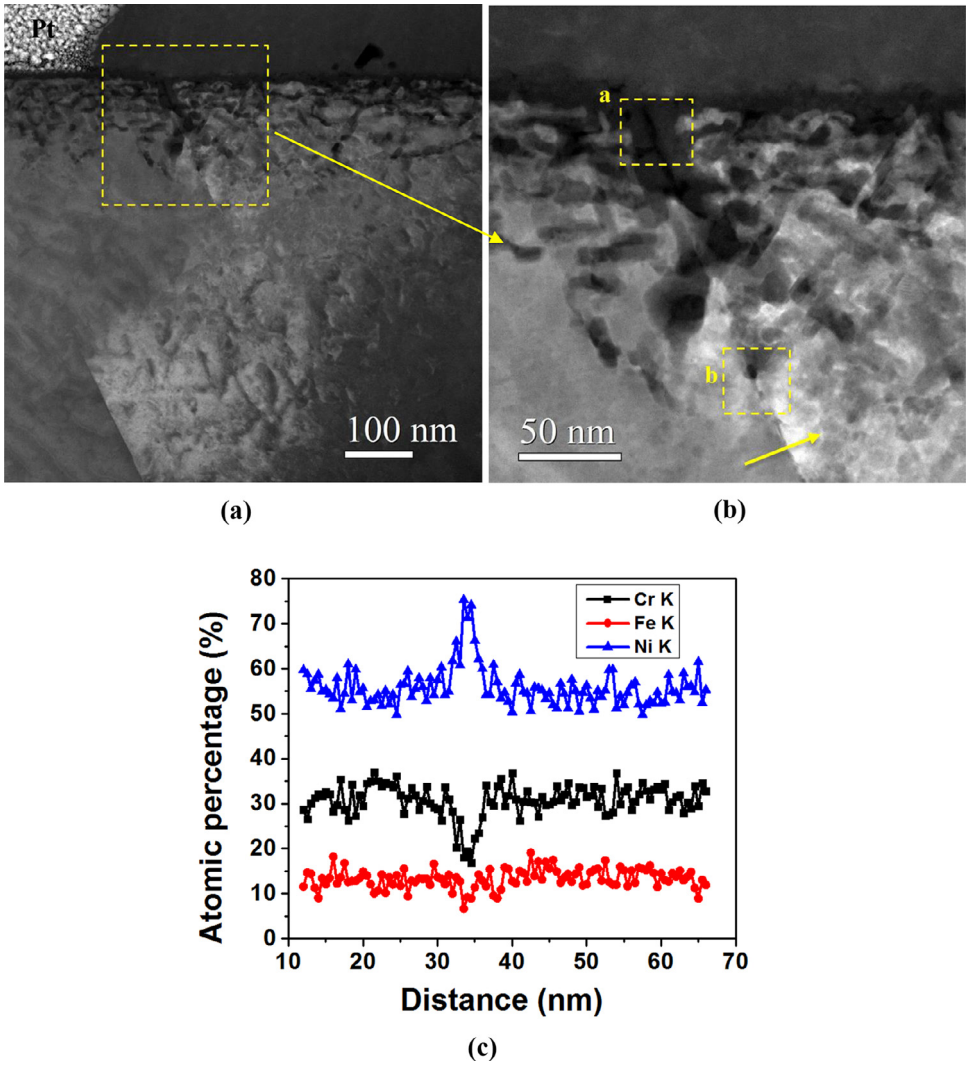

Fig. 7. (a) STEM-HAADF image of the cross section of incoherent twin grain boundary a, (b) enlarged image from the framed area on (a), (c) EDS line profile along the arrow on (b).

4.1. Effect of grain boundary structure on solute diffusivity

A continuous oxide film forms over RHABs in both SA and CR samples (Figs. 2a and 3b), as has been reported in previous work [23,29]. The continuous film is enriched in Cr and is protective [23], in contrast to the penetrative chromia filaments formed in the matrix [25]. The high Cr content and protectiveness is due to the fast supply of Cr via the grain boundary. The Cr from the grain boundary also diffuses along the oxide/matrix interface near the surface/grain boundary intersection which has been reported to be a fast diffusion route [31,32] and promotes the formation of a segment of continuous inner oxide layer in both grains (Figs. 2a and 3b). That explains why the internal oxide gets thinner as it approaches the boundary. Similar results have also been reported on Ni-Cr alloys after high temperature gaseous oxidation [33,34]. The outward diffusion of Cr results in the migration of the grain boundary and the migration zone is depleted in Cr (Figs. 2 and 3). DIGM has been observed not only beneath the surface oxide film [23,29], but also beyond the SCC tips of this alloy [8,16]. So RHABs of alloy 690 can support the rapid diffusion of Cr and are susceptible to migration in high temperature hydrogenated water.

The results from TTBs are consistent with those from RHABs. It should be noted that TTBs were transformed from CTBs as the low-energy grain boundary structure of CTBs was damaged during cold work [22]. TTBs are essentially RHABs and they behave like RHABs.

CTBs behave completely different from RHABs. A thin layer of Cr_2O_3 forms along the CTB with no signs of long-range diffusion of Cr or grain boundary migration (Fig. 4). Consistent results have also been reported in previous work [22]. Therefore, CTBs do not provide a rapid diffusion path of Cr, so there is no boundary migration. Without the formation of a Cr-rich surface oxide film, CTBs are susceptible to the ingress of oxygen to form penetrative Cr_2O_3 as in the grain matrix [25]. The oxidation behavior of CTB is similar to that of grain matrix mainly due to the highly-ordered boundary structure. It should be noted that some transgranular oxide platelets intersect the CTB near the surface (Fig. 5) which could facilitate the diffusion of additional oxygen to CTB along the oxide/metal interfaces [31,32]. That is maybe why the oxide along the CTB looks thicker near the surface.

ITBs have a more disordered interface compared to CTBs, although the orientation relationship between the two grain matrices is the same. A protective oxide film did not form on top of the ITBs either (Figs. 7a and 9d). However, in contrast to CTBs, ITBs show Cr depletion beyond the intergranular oxide. The Cr depletion zone centers around the grain boundary (Figs. 7c and 9e) and no grain boundary migration zone was observed, indicative of

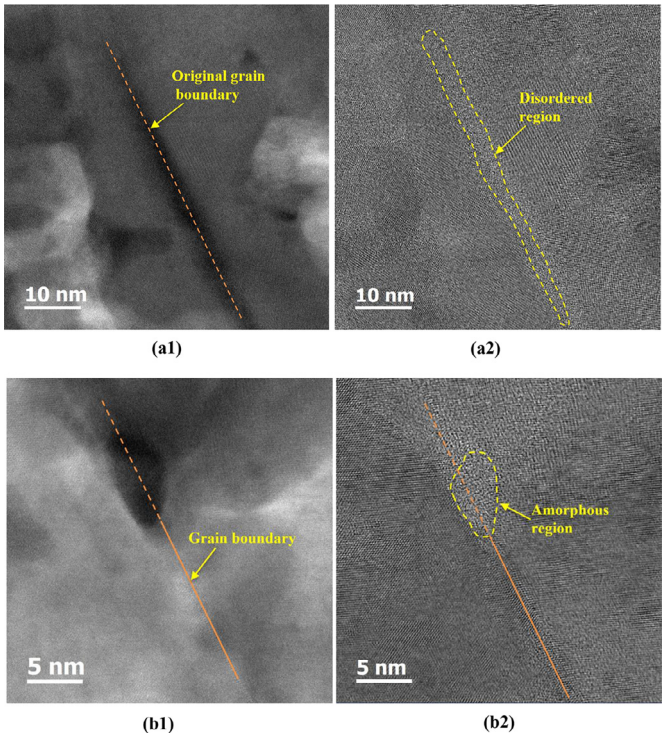

Fig. 8. (a1), (b1) STEM-HAADF and (a2), (b2) bright field images of framed areas on Fig. 7b.

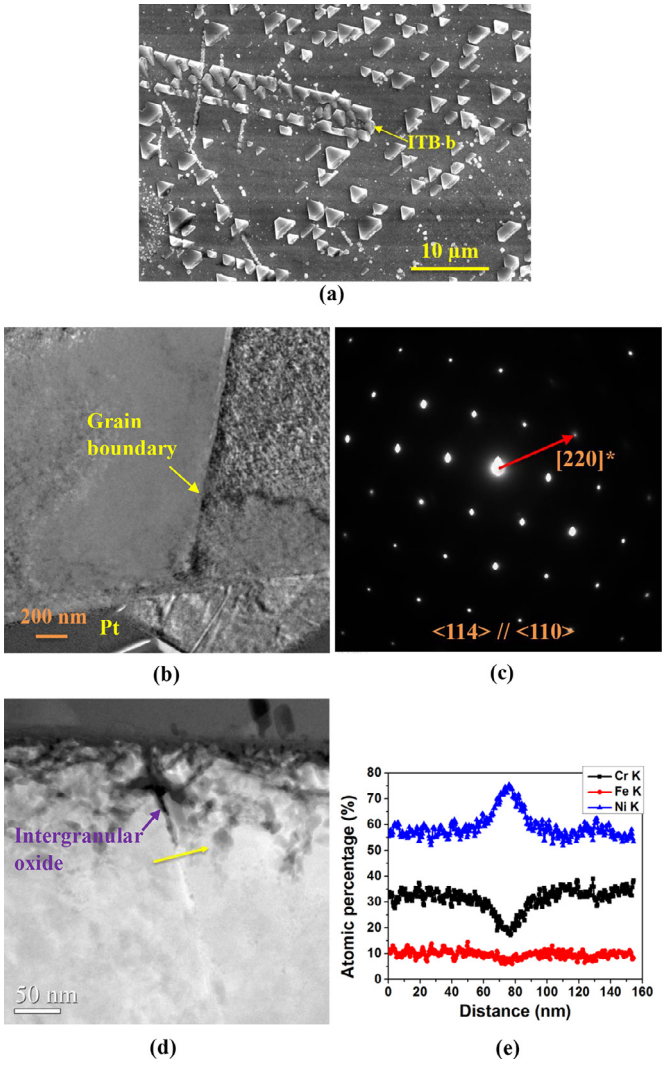

Fig. 9. (a) SEM image of incoherent twin boundary b, (b) TEM micrograph and (c) the corresponding diffraction pattern of the grain boundary, (d) STEM-HAADF image of the cross section and (e) EDS line profile along the arrow in (d).

limited diffusion of Cr. It is concluded that ITBs lie between RHABs and CTBs in term of Cr diffusivity. The Cr diffusion along an ITB is not sufficient to form a continuous oxide film over the boundary (Figs. 7a and 9d), rendering them susceptible to the ingress of oxygen that reacts with the outwards diffusing Cr to form thicker Cr_2O_3 platelets along the boundary (Figs. 7b and 9d).

The diffusivity of Cr is the key factor in the process of intergranular degradation of alloy 690 SA in high temperature hydrogenated water as it determines the ability to form a protective oxide film over the grain boundary, which serves as a barrier against oxygen ingress down the boundary. For alloy 690 SA in high temperature hydrogenated water, the Cr diffusivity along grain boundary decreases in the order of RHABs, ITBs and CTBs. The intergranular diffusion of solute atoms like Cr generally occurs by a vacancy mechanism [35,36]. It has been reported that the grain boundary diffusivity of solute shows a minima at orientations of high coincidence [36–39], and the well accepted explanation is that the highly-ordered grain boundary has larger formation and migration enthalpies of vacancies compared to RHABs [40]. In this work, the orderliness increases from RHABs to ITBs to CTBs, consistent with the decreasing trend of Cr diffusivity. ITBs have the same orientation relationship as CTBs but lose their coherency at the interface. The higher diffusivity of Cr along ITBs compared to CTBs should correspond to its lower density of coincident site in the boundary plane. That may be because the atoms at the coincident sites are confined in both grain lattices and more energy is required for the atoms to break away from the coincident sites. Those coincident atoms would act as pining points during the diffusion process and decrease the diffusivity of solute. Thus, the Cr diffusivity of CTB is the lowest among the sampled grain boundaries, and results in an oxide morphology similar to that in grain matrix. Minkwitz et al. [41] studied the effect of inclination angle of the grain boundary plane with respect to the (111) coherent twin boundary on the diffusivity of Σ3 boundary and also found that the diffusivity decreases with increasing planar density of coincident site in the grain boundary plane. Our recent work [22] and the results from TTB also show that when the grain boundary coherency of CTB in alloy 690 is damaged by cold rolling, the diffusivity of Cr is greatly enhanced, even though the indexes of grain boundary planes are not changed significantly. So, in addition to the orientation relationship, the density of coincident site in grain boundary plane also influences solute diffusivity.

4.2. Effect of grain boundary structure on the microstructure of intergranular oxide

RHABs in alloy 690 are subject to oxidation once the surface oxide film is breached by dynamic straining [7]. From previous work, the intergranular oxide beyond a stagnant SCC crack is composed of a layer of NiO type oxide with mixed cation near the crack and a Cr_2O_3 layer between the NiO layer and the matrix [16]. NiO is thermodynamically stable because the local Ni content is high, and the dissolved hydrogen concentration used here (18 cc H_2/kg H_2O) is below the value corresponding to the Ni/NiO transition (25 cc H_2/kg H_2O) [42]. Both oxides maintain rigid orientation relationships with the parent matrix and there is a clear interface along the original grain boundary within the intergranular oxide [16]. For CTBs, only chromia forms, which also maintains rigid orientation

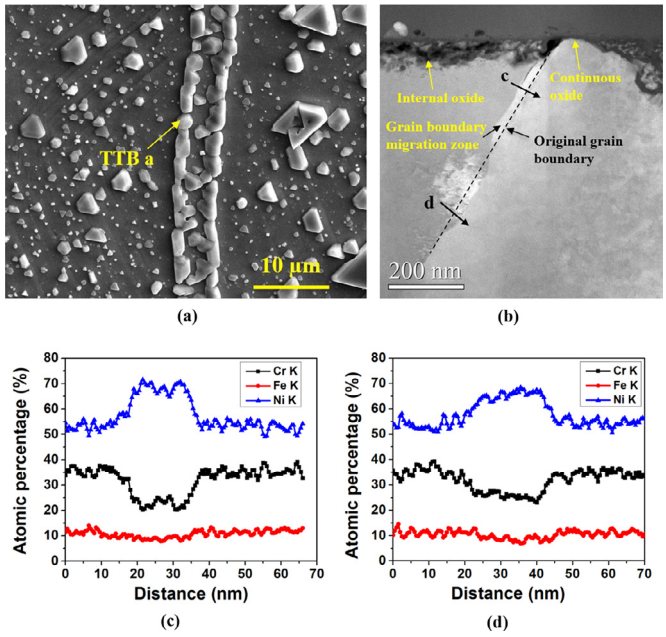

Fig. 10. (a) SEM image of sampled TTB a from cold rolled alloy 690, uniformly strained to 1.9% at 1×10^{-8}/s in 360 °C hydrogenated water after 1650 h, (b) STEM-HAADF image of the cross section and (c) and (d) EDS line profiles along arrows c and d in (b).

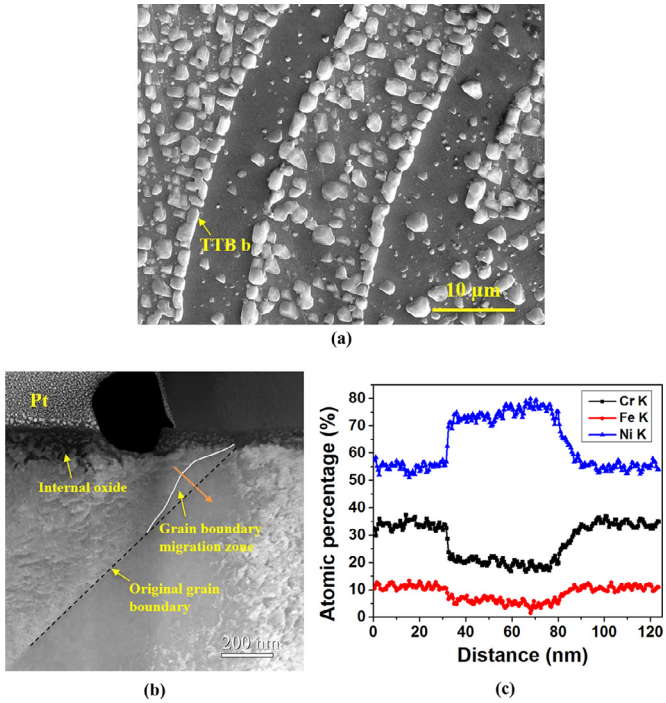

Fig. 11. (a) SEM image of sampled TTB b from cold rolled alloy 690, uniformly strained to 1.9% at 1×10^{-8}/s in 360 °C hydrogenated water after 1650 h, (b) STEM-HAADF image of the cross section and (c) EDS line profile along the arrow in (b).

relationship with either grain matrix (Fig. 5): Cr_2O_3 {006} // substrate {111}, Cr_2O_3 ⟨210⟩ // substrate ⟨110⟩, just like the internal chromia filament formed in the matrix [25]. The major chromia platelet occupies the original grain boundary and maintains such orientation relationship with both grains (Figs. 5b and 5c). That is because chromia tends to develop along the {111} lattice planes of the matrix [25] and both grains share a coherent (111) plane at a CTB. Similar to CTBs, ITBs also support the inward diffusion of oxygen and form intergranular Cr_2O_3 (Figs. 7b and 9d). Nevertheless, there is a disordered and porous interface within the chromia (Fig. 8).

These observations show that the structure of the intergranular oxide is directly related to the structure of the grain boundary. The intergranular degradations of different types of grain boundary are summarized in Fig. 12. For RHABs (Fig. 12a), the fast diffusion of Cr contributes to the formation of a continuous chromia film and results in a Ni-enriched zone. When the surface oxide film is breached, the Ni-enriched metal is exposed to solution and NiO forms. Two sets of NiO layers are epitaxial to their respective parent matrices [16] and the boundary between them should possess the same structure as the original grain boundary. It should be noted that the region of stability of NiO is at a higher potential than that of Cr_2O_3 in the Pourbaix diagram [42]. The oxygen concentration decreases as it diffuses through the NiO layer until Cr_2O_3 becomes stable and forms. As the chromia also maintains a rigid orientation relationship with the parent grain matrix, the interface structure should also inherit from the original grain boundary structure. Only Cr_2O_3 was observed along CTBs and ITBs due to the much lower diffusivity of Cr (Figs. 12a and 12b). Oxygen diffuses into the boundaries at the beginning as there is no protective surface oxide film and the local Cr content is high enough to form Cr_2O_3. The limited outward Cr diffusion along ITBs promotes the formation of a thicker chromia platelet and causes Cr depletion along the grain boundary (Fig. 12b). Cr is nearly immobile along CTB and only oxygen diffuses inwards as in the grain matrix (Fig. 12c). It has been revealed that the interface between Cr_2O_3 {006} and substrate {111} is semi-coherent [25]. Accordingly, the intergranular oxides formed in CTBs possess an ordered interface structure due to the perfect coherent grain boundary structure while the oxides along ITBs show a defective interface since the ITBs have lost coherency.

It is interesting to find that the results in this work are contradictory to all the previous work which suggest that twin boundaries have significantly higher resistance to intergranular oxidation than RHABs. Those works cover gaseous oxidation of Ni-40 at.%Fe (at 1000 °C) [17], Ni-base alloy 718 (at 900 °C) [43], ferritic stainless steel (at 650 °C) [44] and aqueous oxidation of alloy 600 in simulated PWR primary water [18]. The work on the aqueous oxidation of alloy 600, which is more relevant to this study, showed that the twin boundary of alloy 600 was not oxidized at all [18]. As to RHABs, they are susceptible to intergranular oxidation in alloy 600 [18,29,45–47] while in alloy 690, a protective surface film forms and prevents the ingress of oxygen (Fig. 2a) [23,29]. The higher SCC resistance of alloy 690 compared to alloy 600 is probably due to its ability to form such a protective oxide film over RHABs. It seems that the grain boundary structure dependence of intergranular oxidation susceptibility is strongly influenced by the chemical composition of the alloy which is beyond the scope of this work.

4.3. Effect of grain boundary structure on the SCC resistance

It is surprising that CTBs in alloy 690 are almost immune to SCC initiation [22] although they are susceptible to intergranular oxidation. On the contrary, RHABs can form a protective surface oxide film but are subject to crack initiation during dynamic straining [7,22]. It is likely that the strength of the oxidized grain boundary is closely linked to the structure of the intergranular oxide. It has been reported that the intergranular oxide/matrix interface can serve as a route for crack initiation [48]. As mentioned above, the chromia formed along CTBs maintains semi-coherency with both grains. Such an interface is highly ordered and normally has relatively high strength and can easily accommodate the movement of dislocations. Thus, it still possesses a high resistance to

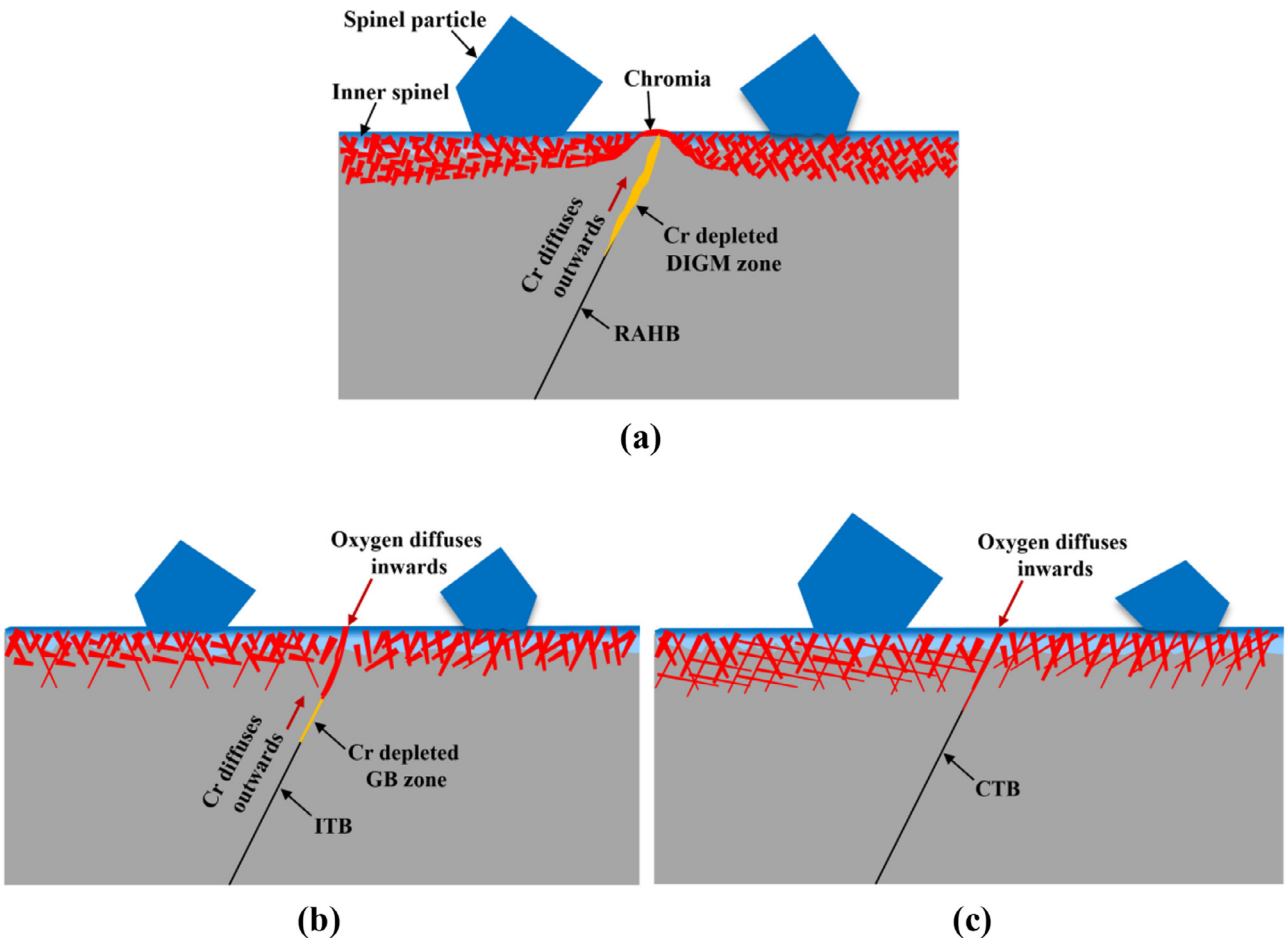

Fig. 12. Schematics of intergranular degradation of (a) RHAB, (b) ITB and (c) CTB.

crack initiation. As for RHABs, the surface oxide film cannot be sustained during dynamic straining and the intergranular oxides formed thereafter inherit a random high angle boundary structure from the original grain boundaries [16]. The random high angle boundary within the intergranular oxide is much less ordered and is more susceptible to SCC initiation. In previous work [22], it has been reported that CTBs could be transformed to TTBs by cold rolling, which were susceptible to SCC initiation. So, for a given alloy, the SCC initiation resistance is dictated by the grain boundary structure.

Understanding how the intergranular SCC resistance is related to the grain boundary structure is crucial to identifying the most susceptible grain boundary to cracking, and predicting the safety margin of components in service. From this work, it is determined that the grain boundary structure of alloy 690 can significantly affect the diffusivity of solute and determine the structure of the intergranular oxide, which is closely related to the cracking resistance. For RHABs, the grain boundary structure can be further characterized by its ability to accommodate the slip systems in the neighboring grains, which correlates with the local stress and strain distributions [49,50]. It has been reported that the slip discontinuity across the grain boundary raises the local stress and increases the intergranular cracking susceptibility of irradiated austenitic stainless steel in high temperature water [51,52]. However, local stress concentration cannot account for the intergranular cracking by itself as the grain boundary normally does not crack without the effect of environment. The local stress and strain states may also influence the intergranular oxidation process. It has been reported that the strain heterogeneity near the grain boundary can enhance the intergranular oxidation rate of alloy 82 in simulated PWR primary water [53]. For the RHABs of alloy 690, prior to the occurrence of intergranular oxidation, the breach of the surface oxide film is a key step in the process of SCC initiation and should also be closely related to the dislocation/grain boundary interaction which is dictated by the grain boundary structure. To fully understand the role of grain boundary structure in the intergranular SCC process, the structure dependences of corrosion process and local stress/strain condition near the boundary should be both considered.

5. Conclusions

In this work, the environmental degradation behaviors of four different grain boundaries: random high angle boundaries (RHABs), coherent twin boundaries (CTBs), incoherent twin boundaries (ITBs), and transformed twin boundaries (TTBs) prior to crack initiation were investigated on alloy 690 following slow strain rate tensile tests in 360 °C hydrogenated water. RHABs and TTBs provide fast diffusion paths for Cr and undergo grain boundary migration, while CTBs show little outward diffusion of Cr and no migration. ITBs show Cr depletion but no migration. The Cr diffusivity along grain boundary correlates closely with the density of coincident site in the grain boundary plane and dictates the morphology of oxide formed near the grain boundary. The fast Cr diffusion along RHABs and TTBs promotes the formation of a continuous surface oxide film over the boundaries. While for CTBs and ITBs, the Cr diffusion is not fast enough to support the formation of such continuous oxide film and intergranular oxide forms instead.

The stress corrosion cracking (SCC) resistance of the grain boundary is closely related to the structure of the intergranular oxide. CTBs are highly resistant to cracking because the intergranular chromia maintains semi-coherency with the grain matrices. Once the continuous oxide film over a RHAB is breached during dynamic straining, the intergranular oxide inherits the highly-disordered boundary structure from the original grain boundary and becomes susceptible to cracking. For a given alloy, the SCC resistance is dictated by the grain boundary structure due to its effects on the corrosion process and the local stress-strain state.

Declaration of Competing Interest

None.

Acknowledgements

The work was supported through the DOE I-NERI program contract 2011-01-K. The authors would like to thank Young Suk Kim and Sung Soo Kim from Korea Atomic Energy Research Institute for providing the materials for this study, and Alex Flick from the University of Michigan, and the Irradiated Materials Testing Laboratory at the University of Michigan. Wenjun Kuang acknowledges the support of Young Talent Support Plan of XJTU.

Reference

[1] K. Smith, A. Klein, P. Saint-Paul, J. Blanchet, Inconel 690: a material with improved corrosion resistance for PWR steam generator tubes, in: Proceedings of the Second International Symposium on Environmental Degradation of Materials in Nuclear Power Systems-Water Reactors, Monterey, California, American Nuclear Society, 1985.
[2] K. Norring, J. Engstrom, P. Norberg, Intergranular stress corrosion cracking in steam generator tubing. testing of alloy 690 and alloy 600 tubes, in: Proceedings of the 3rd International Symposium Environmental Degradation of Materials in Nuclear Power Systems, Traverse city, Michigan, Water Reactors, 1987.
[3] J.J. Kai, C.H. Tsai, G.P. Yu, The IGSCC, sensitization, and microstructure study of alloys 600 and 690, Nucl. Eng. Des. 144 (1993) 449–457.
[4] M.B. Toloczko, S.M. Bruemmer, Cack growth response of alloy 690 in simulated pwr primary water, in: Proceedings of the 14th International Conference on Environmental Degradation of Materials in Nuclear Power Systems, Virginia Beach, VA, 2009.
[5] M.B. Toloczko, M.J. Olszta, S.M. Bruemmer, One dimentional cold rolling effects on stress corrosion crack growth in alloy 690 tubing and plate materials, in: Proceedings of the 15th International Conference on Environmental Degradation of Materials in Nuclear Power Systems-water reactors, Colorado Springs, Colorado, USA, 2011.
[6] P.L. Andresen, M.M. Morra, K. Ahluwalia, Effect of deformation temperature, orientation and carbides on scc of alloy 690, in: Proceedings of the 16th International Conference on Environmental Degradation of Materials in Nuclear Power Systems-Water Reactors, Asheville, North Carolina, USA, 2013.
[7] T. Moss, W. Kuang, G.S. Was, Stress corrosion crack initiation in alloy 690 in high temperature water, Curr. Opin. Solid State Mater. Sci. 22 (2018) 16–25.
[8] T. Moss, G.S. Was, Accelerated stress corrosion crack initiation of alloys 600 and 690 in hydrogenated supercritical water, Metall. Mater. Trans. A 48 (2017) 1613–1628.
[9] J. M.Boursier, F. Vaillant, P. Saulay, Y. Brechet, G. Zacharie, Effect of the strain rate on the stress corrosion cracking in high temperature primary water: comparison between the alloys 690 and 600, in: Proceedings of the 11th International Conference Environmental Degradation of Materials in Nuclear Systems, Stevenson, WA, 2003.
[10] W. Kuang, C. Miller, M. Kaufman, T. Alam, B. Gwalani, R. Banerjee, Effects of cold work and aging treatments on the microstructure and stress corrosion cracking initiation behavior of solution annealed alloy 690, in: Proceedings of the 17th International Conference on Environmental Degradation of Materials in Nuclear Power Systems-water reactors, Ottawa, Ontario, Canada, 2015.
[11] T. Moss, G.S. Was, Accelerated stress corrosion crack initiation of alloy 690 and alloy 600 in high temperature hydrogenated water, in: Proceedings of the 6th International Conference on Environmental Degradation of Materials in Nuclear Power Systems-Water Reactors, Asheville, North Carolina, USA, 2013.
[12] W. Kuang, G.S. Was, The effects of grain boundary carbide density and strain rate on the stress corrosion cracking behavior of cold rolled alloy 690, Corros. Sci. 97 (2015) 107–114.
[13] K. Arioka, T. Terachi, Degradation of alloy 690 after relatively short times, Corrosion 72 (2016) 1252–1268.
[14] Z. Zhai, M. Toloczko, K. Kruska, S. Bruemmer, Precursor evolution and stress corrosion cracking initiation of cold-worked alloy 690 in simulated pressurized water reactor primary water, Corrosion 73 (2017) 1224–1236.
[15] W. Kuang, G.S. Was, A high-resolution characterization of the initiation of stress corrosion crack in alloy 690 in simulated pressurized water reactor primary water, Corros. Sci. (2019) 108243.
[16] W. Kuang, M. Song, G.S. Was, Insights into the stress corrosion cracking of solution annealed alloy 690 in simulated pressurized water reactor primary water under dynamic straining, Acta Mater 151 (2018) 321–333.
[17] S. Yamaura, Y. Igarashi, S. Tsurekawa, T. Watanabe, Structure-dependent intergranular oxidation in Ni–Fe polycrystalline alloy, Acta Mater. 47 (1999) 1163–1174.
[18] Y.S. Lim, S.W. Kim, S.S. Hwang, H.P. Kim, C. Jang, Intergranular oxidation of Ni-based alloy 600 in a simulated PWR primary water environment, Corros. Sci. 108 (2016) 125–133.
[19] Y. Pan, B.L. Adams, T. Olson, N. Panayotou, Grain-boundary structure effects on intergranular stress corrosion cracking of alloy X-750, Acta Mater. 44 (1996) 4685–4695.
[20] V.Y. Gertsman, S.M. Bruemmer, Study of grain boundary character along intergranular stress corrosion crack paths in austenitic alloys, Acta Mater. 49 (2001) 1589–1598.
[21] K.J. Leonard, M.N. Gussev, J.N. Stevens, J.T. Busby, Analysis of stress corrosion cracking in alloy 718 following commercial reactor exposure, J. Nucl. Mater. 466 (2015) 443–459.
[22] W. Kuang, G.S. Was, C. Miller, M. Kaufman, T. Alam, B. Gwalani, R. Banerjee, The effect of cold rolling on grain boundary structure and stress corrosion cracking susceptibility of twins in alloy 690 in simulated pressurized water reactor primary environment, Corros. Sci. 130 (2018) 126–137.
[23] M.J. Olszta, D.K. Schreiber, M.B. Toloczko, S.M. Bruemmer, Alloy 690 surface nanostructures during exposure to PWR primary water and potential influence on stress corrosion crack initiation, in: Proceedings of the 16th international Conference on Environmental Degradation of Materials in Nuclear Power Systems-Water Reactors, Asheville, North Carolina, USA, 2013.
[24] W. Kuang, G.S. Was, The effects of strain rate and carbon concentration on the dynamic strain aging of cold rolled Ni-based alloy in high temperature water, Scripta Mater. 107 (2015) 107–110.
[25] W. Kuang, M. Song, P. Wang, G.S. Was, The oxidation of alloy 690 in simulated pressurized water reactor primary water, Corros. Sci. 126 (2017) 227–237.
[26] W.J. Kuang, E.H. Han, X.Q. Wu, J.C. Rao, Microstructural characteristics of the oxide scale formed on 304 stainless steel in oxygenated high temperature water, Corros. Sci. 52 (2010) 3654–3660.
[27] W. Kuang, X. Wu, E.-H. Han, J. Rao, The mechanism of oxide film formation on alloy 690 in oxygenated high temperature water, Corros. Sci. 53 (2011) 3853–3860.
[28] W.J. Kuang, X.Q. Wu, E.H. Han, Influence of dissolved oxygen concentration on the oxide film formed on alloy 690 in high temperature water, Corros. Sci. 69 (2013) 197–204.
[29] T. Moss, G. Cao, G.S. Was, Oxidation of alloy 600 and alloy 690: experimentally accelerated study in hydrogenated supercritical water, Metall. Mater. Trans. A (2017) 1–17.
[30] M.J. Olszta, D.K. Schreiber, L.E. Thomas, S.M. Bruemmer, Penetrative internal oxidation from alloy 690 surface and stress corrosion crack walls during exposure to pwr primary water, in: Proceedings of the 15th International Conference on Environmental Degradation of Materials in Nuclear Power Systems-Water Reactors, Colorado Springs, Colorado, USA, 2011.
[31] D.P. Whittle, Y. Shida, G.C. Wood, F.H. Stott, B.D. Bastow, Enhanced diffusion of oxygen during internal oxidation of nickel-base alloys, Philos. Mag. A 46 (1982) 931–949.
[32] A. Martínez-Villafañe, F.H. Stott, J.G. Chacon-Nava, G.C. Wood, Enhanced oxygen diffusion along internal oxide–metal matrix interfaces in Ni–Al alloys during internal oxidation, Oxid. Met. 57 (2002) 267–279.
[33] G.C. Wood, F.H. Stott, D.P. Whittle, Y. Shida, B.D. Bastow, The high-temperature internal oxidation and intergranular oxidation of nickel-chromium alloys, Corros. Sci. 23 (1983) 9–25.
[34] K. Kruska, D.K. Schreiber, M.J. Olszta, B.J. Riley, S.M. Bruemmer, Temperature-dependent selective oxidation processes for Ni-5Cr and Ni-4Al, Corros. Sci. 139 (2018) 309–318.
[35] E.P. Simonen, L.E. Thomas, S.M. Bruemmer, Diffusion kinetic issues during intergranular corrosion of Ni-base alloys, in: Proceedings of the NACE International Corrosion 2000, 2000.
[36] P. Klugkist, A.N. Aleshin, W. Lojkowski, L.S. Shvindlerman, W. Gust, E.J. Mittemeijer, Diffusion of Zn along tilt grain boundaries in Al: pressure and orientation dependence, Acta Mater. 49 (2001) 2941–2949.
[37] X.M. Li, Y.T. Chou, High angle grain boundary diffusion of chromium in niobium bicrystals, Acta Mater. 44 (1996) 3535–3541.
[38] T. Surholt, D.A. Molodov, C. Herzig, Orientation dependence of Ge diffusion along symmetrical [111]tilt grain boundaries in Al, Acta Mater. 46 (1998) 5345–5355.
[39] E. Budke, T. Surholt, S.I. Prokofjev, L.S. Shvindlerman, C. Herzig, Tracer diffusion of Au and Cu in a series of near Σ=5 (310)[001]symmetrical Cu tilt grain boundaries, Acta Mater. 47 (1999) 385–395.
[40] B.B. Straumal, L.M. Klinger, L.S. Shvindlerman, The effect of crystallographic parameters of interphase boundaries on their surface tension and parameters of the boundary diffusion, Acta Metall. 32 (1984) 1355–1364.
[41] C. Minkwitz, C. Herzig, E. Rabkin, W. Gust, The inclination dependence of gold tracer diffusion along a Σ3 twin grain boundary in copper, Acta Mater. 47 (1999) 1231–1239.
[42] B. Beverskog, I. Puigdomenech, Pourbaix diagrams for the ternary system of iron-chromium-nickel, Corrosion 55 (1999) 1077–1087.

[43] S.L. Yang, U. Krupp, H.J. Christ, V. Braz Trindade, The relationship between grain boundary character and the intergranular oxide distribution in IN718 superalloy, Adv. Eng. Mater. 7 (2005) 723–726.
[44] M.P. Phaniraj, D.-.I. Kim, Y.W. Cho, Effect of grain boundary characteristics on the oxidation behavior of ferritic stainless steel, Corros. Sci. 53 (2011) 4124–4130.
[45] G. Bertali, M.G. Burke, F. Scenini, N. Huin, The effect of temperature on the preferential intergranular oxidation susceptibility of alloy 600, Metall. Mater. Trans. A. 49 (2018) 1879–1894.
[46] R.A. Morris, N. Lewis, D.S. Morton, 3D analysis of surface treatment effects on the oxidation of grain boundaries in alloy 600, in: Proceedings of the 16th International Conference on Environmental Degradation of Materials in Nuclear Power Systems-Water Reactors, Asheville, North Carolina, USA, 2013.
[47] L. Fournier, O. Calonne, P. Combrade, P. Scott, P. Chou, R. Pathania, Grain boundary oxidation and embrittlement prior to crack initiation in alloy 600 in PWR primary water, in: Proceedings of the 15th International Conference on Environmental Degradation of Materials in Nuclear Power Systems-water reactors, Colorado Springs, Colorado, USA, 2011.
[48] H. Dugdale, D.E.J. Armstrong, E. Tarleton, S.G. Roberts, S. Lozano-Perez, How oxidized grain boundaries fail, Acta Mater. 61 (2013) 4707–4713.
[49] W.Z. Abuzaid, M.D. Sangid, J.D. Carroll, H. Sehitoglu, J. Lambros, Slip transfer and plastic strain accumulation across grain boundaries in Hastelloy X, J. Mech. Phys. Solids. 60 (2012) 1201–1220.
[50] Y. Guo, T.B. Britton, A.J. Wilkinson, Slip band–grain boundary interactions in commercial-purity titanium, Acta Mater. 76 (2014) 1–12.
[51] E.A. West, G.S. Was, Strain incompatibilities and their role in intergranular cracking of irradiated 316L stainless steel, J. Nucl. Mater. 441 (2013) 623–632.
[52] M.D. McMurtrey, B. Cui, I. Robertson, D. Farkas, G.S. Was, Mechanism of dislocation channel-induced irradiation assisted stress corrosion crack initiation in austenitic stainless steel, Curr. Opin. Solid State Mater. Sci. 19 (2015) 305–314.
[53] M. Wehbi, T. Couvant, C. Duhamel, J. Crepin, Oxidation of nickel-base welds 182 and 82 in simulated primary water of pressurised water reactors, Mater. High Temp. 32 (2015) 1–9.

View publication stats